The International Journal of Advanced Manufacturing Technology (2019) 101:2027–2036
https://doi.org/10.1007/s00170-018-3035-1

ORIGINAL ARTICLE

Conceptual design, control, and simulation of a 5-DoF robotic manipulator for direct additive manufacturing on the internal surface of radome systems

Stanislao Grazioso[1] · Manuele Di Maio[1] · Giuseppe Di Gironimo[1]

Received: 13 April 2018 / Accepted: 12 November 2018 / Published online: 27 November 2018

Abstract
In this paper, a novel concept of robotic manipulator is developed for direct additive manufacturing on non-planar surfaces. The application scenario is the metal coating of the internal surface of radome systems, using frequency selective surface patterns. The manipulator is presented from the design, modeling, and control point of view. It is developed following an application-driven approach, meaning that the requirements from the application and the additive manufacturing technology are translated into the design specifications of the robotic system. Simulation results demonstrate that the proposed control strategy based on a decentralized architecture is satisfactory to accurately control the motion of the robotic mechanisms along the trajectory foresees by the direct additive manufacturing task.

Keywords Additive manufacturing · Aerosol jet printing · Design method · Virtual prototyping · Robot control

1 Introduction

Direct writing technologies refer to additive manufacturing processes which can create two– or three– dimensional functional structures directly on flat or conformal surfaces in complex shapes, without any tooling or masks [1]. The peculiarity of these novel technologies is their ability to build freeform structures with feature resolution in one or more dimensions below 50μm [2], which is particularly appealing in the context of micromanufacturing [3, 4]. As a matter of fact, the possibility to build homogeneous, compact, accurate and freeform patterns makes this class of technologies attractive for metal coating of complex non–planar objects, to enhance the electromechanical properties of the substrate. However, specific industrial applications might require the coating of surfaces which are difficult to reach. This is pushing technologists and roboticists towards the design of custom and application–oriented robotics systems able to enable the development of such additive manufacturing technologies in hazardous industrial domains.

✉ Stanislao Grazioso
stanislao.grazioso@unina.it

[1] Department of Industrial Engineering, University of Naples Federico II, 80125, Napoli, Italy

In this paper, we present the design, modeling, and control of a five degrees–of–freedom (DoF) robotic manipulator for direct additive manufacturing on a specific curved surface. The industrial scenario behind this work is the metal coating of the internal surface of a double-curvature object, namely the radome, a structural and weatherproof enclosure that protects a microwave (e.g., radar) antenna in aircrafts and missile systems. The radome is constructed of material that minimally attenuates the electromagnetic signals transmitted or received by the antenna. The motivation which leverages this work is the enhancement of the transmission of radio signals made possible by coating the internal surface of the radome using appropriate metallic patterns. To this end, frequency selective surfaces (FSS) [5] are built to improve the band-pass filtering properties of the aerospace components carrying antennas. Typical requirements of FSS for aerospace applications are: thicknesses between 10 and 50 μm and accuracy below 1 μm. This work is part of a broader project, focused on manufacturing of radome and radar antenna systems [6–8].

Many manufacturing coating technologies exist for guarantee the FSS requirements, as thermal spray [9, 10] or physical and chemical vapor deposition [11, 12]. However, the majority of these technologies deposits a full layer of material, usually on planar surfaces. The problems in our context are (i) the FSS pattern is usually complex, meaning that the radome substrate will have coated and

non-coated regions; (ii) the FSS pattern must be built on non-planar surfaces. Thus, adopting one of the classical manufacturing technologies requires masking the internal surface of the radome. Moreover, these technologies are difficult to implement with ad-hoc robotic systems, which eventually might be used to coat only selected regions of the mechanical component.

For these reasons, our idea is to use additive manufacturing technologies to build FSS patterns. In particular, we select the aerosol jet printing (AJP) technology, for the mechanical and electrical properties of the resulting coating that it is able to guarantee [13]. Aerosol jet printing is able to built free–form metal patterns with thicknesses between 1 μm to mm (multi–layers). Furthermore, it is a non-contact technology which allows depositing a large set of materials on a large set of substrates (also non–planar), without the need of masking.

Since the overall internal surface of the radome is difficult–to–reach with standard robotic machines, we develop a novel concept of robotic manipulator with 5 DoF. The robotic manipulator is designed from the mechanical and control point of view. The design parameters are selected from the requirements needed to implement AJP. The kinematics and dynamics models of the manipulator are developed for simulation purposes. An independent joint control scheme is proposed as possible solution for the motion control of the manipulator. The results, in terms of position errors along the trajectories which allow to build a test FSS pattern, are promising towards an hardware implementation of the simulated controlled system.

This paper is organized as follows. In the rest of this section, we provide an overview of additive manufacturing technologies which can be used for metal coating of non–planar surfaces, focusing on AJP, and we show the main contributions of the current work. In Section 2, the methodology used in the paper is presented. Section 3 relates with the mechanical description of the manipulator, whose kinematic and dynamic models are presented in Section 4. The control system design is addressed in Section 5, while simulations are presented in Section 6. Section 7 concludes the paper and discusses future developments.

1.1 Direct additive manufacturing

Additive manufacturing technologies refer to processes which allow to create freeform geometrical structures through adding material layer by layer [14–16]. These technologies can be grouped in: photopolymerization processes, extrusion–based systems, powder bed fusion processes, material and binder jetting, sheet lamination processes and direct write technologies (or direct additive manufacturing) [2]. Among these processes, the latter have been selected as the most promising for the metal coating of FSS patterns, on existing non-planar surfaces [17]. As a matter of fact, direct additive manufacturing technologies are able to build freeform structures on substrates using an appropriate deposition tool. The most diffuse approach to direct writing involves the use of liquid inks suspended as an aerosol mist [18]. These inks are deposited on a surface and contain the basic materials which will eventually become the desired structure. The commercialized and patented version of this approach is the AJP process developed by Optomec [13, 19]. The AJP process begins with the atomization of the liquid ink material so that a dense aerosol flow of tiny droplets 1-5 μm in size is created. The generated aerosol is delivered to the deposition head using a carrier gas, usually nitrogen. Within the deposition head, the aerosol is focused through a coaxial sheat air flow, and the resulting high-velocity steam exits the chamber through an orifice directed towards the substrate. The beam width depends on the ratio between sheat gas and aerosol flow as well as on the distance nozzle–substrate: the flux results more collimated as the sheat gas increases and the distance decreases. A schematic illustration of the AJP process is shown in Fig. 1. One benefit of a collimated aerosol spraying process is its high stand–off distance and large working distance from the substrate. Indeed, a good adhesion of the particles is achieved if the deposition head is positioned between 1 to 5 mm from the substrate, with an angle between its axis and the tangent to the non–planar surface of the substrate between ± 60 degrees [18]. This feature mostly motivates the use of AJP for the metal coating of the internal surface of the radome. An improvement to this technology can be found in the recent patent on the use of a convergent–divergent–convergent nozzle, instead of a classical convergent nozzle, for obtaining a more collimated and high velocity beam [20]. This process is referred to as collimated aerosol beam direct write (CAB-DW). The enhanced AJP allows reducing the length of the deposition line of 62% on planar surfaces and of 67% on discontinuous surfaces, as surfaces presenting a curvature change [18].

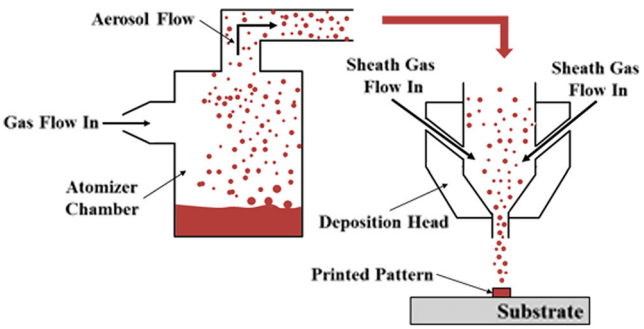

Fig. 1 Aerosol jet printing process (image adapted from [13])

To date, AJP has been mainly used for electronic applications [21–23]. Our idea is to bring the advantages of this technology to enable the metal coating of the internal surface of the radome, which is an high challenge application required by our aerospace industrial partner. However, the first step in enabling it relates to studies and developments of concepts which might be eventually used as deposition head in this context. This represents the major topic of this paper.

1.2 Main contributions

The main contributions of the current work are listed as follows:

1. Aerosol Jet Printing used as additive manufacturing technology for building FSS pattern on radome systems.
2. Application–driven methodology for design and simulation of robotic systems, including mechanical design, kinematic and dynamic modeling, control system strategy.
3. Design of a compact 2-DoF wrist mechanism for orientation purposes in confined spaces.
4. Indipendent Joint Control architecture to ensure the position accuracy required in metal coating applications through additive manufacturing.

2 Methodology

The application-driven methodology used in this paper is summarized in Fig. 2. The requirements on the properties of the coating and the FSS pattern motivates the use of AJP as additive manufacturing technology. The mechanical design of the robotic manipulator takes into account the confined environment on which it will work and the design requirements from the technology (1 to 5 mm from the substrate with an angle of ±60 degrees; accuracy below 1 μm for the FSS pattern). Then, the mechanical design is validated through the dynamic and control simulations. The kinematic model of the manipulator and a classic motion profile are used to generate the inverse kinematic mapping, and thus the joint trajectories. The joint torques are obtained solving the inverse dynamics of the manipulator. This analysis is used to size the actuators needed for generate the motion required from the FSS pattern. The parameters of the controllers are tuned such that the controlled system is stable and the errors along the reference trajectory are small. The tuning process is iterated until the tracking error of the manipulator along the reference trajectory, as the difference between the desired and the actual trajectory is below 10^{-3}.

3 Mechanics

The mechanical design of the robotic manipulator has been driven by the considered application, i.e., the metal coating of the internal surface of the radome, using the aerosol-jet printing as direct additive manufacturing technology. In the design phase, we consider the coating of the worst–case radome, which has an high h of 500 mm and a base diameter $2r$ equal to 200 mm (see, e.g., Fig. 4). The control system should:

1. Ensure the motion and the correct positioning of the nozzle inside the radome. The optimal deposition is achieved when the distance between the nozzle and the radome surface is from l_1 =1 mm to l_2 =5 mm with an angle α in the range ±60° between the tangent at the coating application point and the direction of the aerosol jet. Figure 3 shows the optimal workspace for aerosol jet operations on the internal surface of the radome.

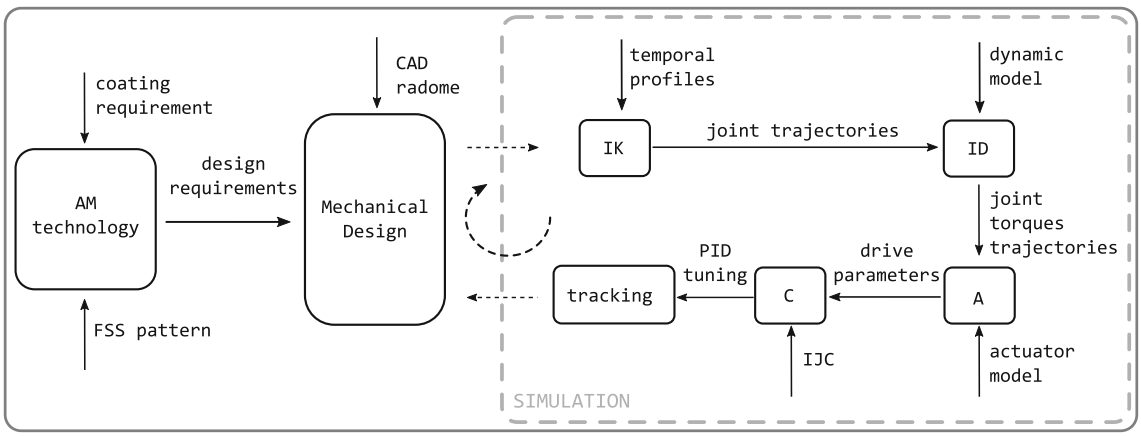

Fig. 2 The application-driven methodology for developing mechatronic systems used in the paper. Starting from the left: *AM* = additive manufacturing; *IK* = inverse kinematics; *ID* = inverse dynamics; *A* = actuator; *C* = control; *IJC* = indipendent joint control

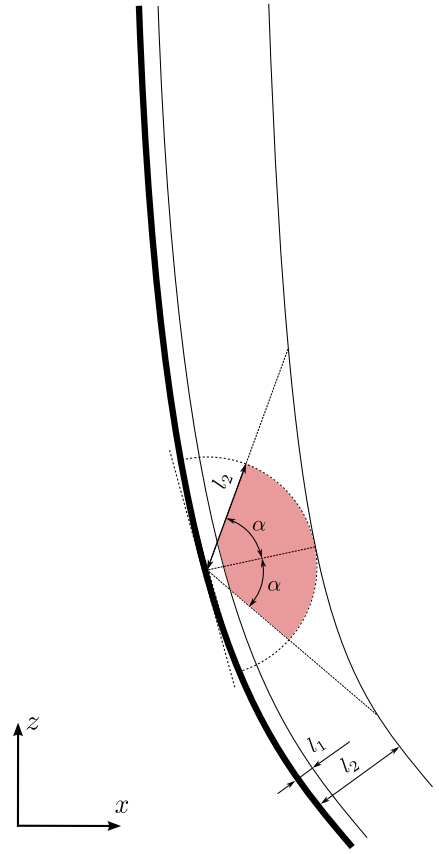

Fig. 3 Planar optimal workspace for aerosol jet printing operations on the internal surface of the radome. This workspace is obtained by cutting the radome with one of the member of the bundle of planes obtained from the vertical axis of the radome and orthogonal to the base of the radome itself. The red region is the optimal workspace wherein the nozzle should be located during the operations

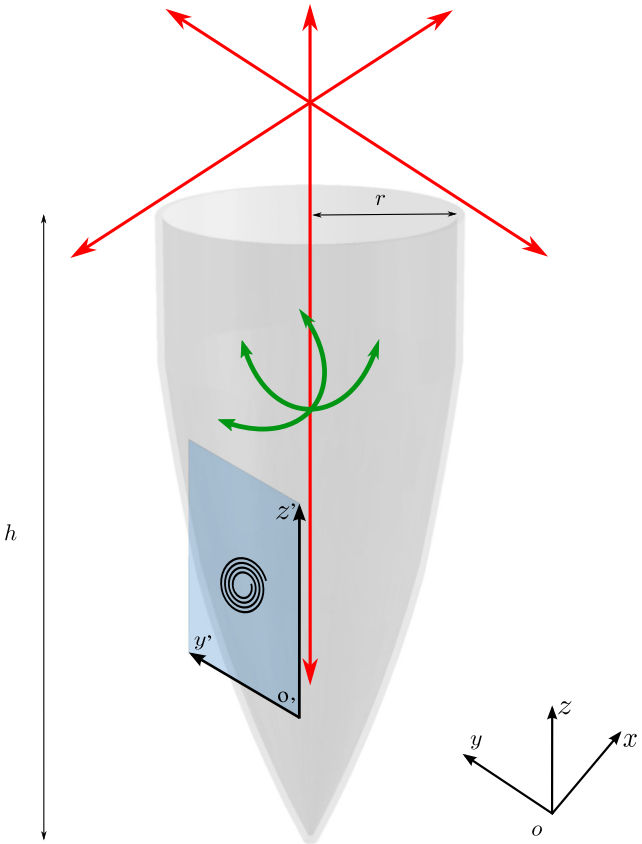

Fig. 4 Conceptual placement of the manipulator axes (three prismatic, red and two revolute, green joints) in the internal surface of the radome and example of FSS pattern in the plane y'z'

2. Guarantee high accuracy in the nozzle positioning, with a tracking errors along the reference trajectory below 10^{-3}.

From these requirements, the following design specifications for the robotic system have been obtained.

1. Five degrees-of-freedom (DoF) kinematic mechanism.
2. Telescopic joint with 600 mm stroke along the vertical axis of the radome, from now on referred to as z axis.
3. Two prismatic joints with 300 mm stroke along two planar axis perpendicular to z axis, such that they constitute a laevogyrate reference frame, from now on referred as x and y axes.
4. One revolute joint to allow the rotation of the nozzle about the z axis. From now on, we will refer to the nozzle also as end-effector.
5. One revolute joint to allow the rotation about the y axis of the end-effector.

Figure 4 shows the conceptual placement of the joints for a suitable 5-DoF mechanism and the axis nomenclature. It is important to notice the importance of a fixture system for the radome, able to guarantee a stable alignment of the vertical axis of the radome with the z axis of the robotic manipulator. In the following we present the final concepts of robotic manipulator and fixture system, as selected through a group decision making session [24, 25] which involved the three authors of the current work.

3.1 Robotic manipulator

The robotic manipulator has a 5–DoF mechanical structure, which allows to locate the nozzle in the workspace. Three translational axis allow to position the nozzle, whose orientation is ensured by a compact 2–DoF mechanism. The motion along x and y axis is obtained using a classical planar cartesian mechanical structure. In particular, the motion along the z axis is generated using a linear–motion telescopic mechanism [26]. This mechanism includes a plurality of block members which can elongate and contract,

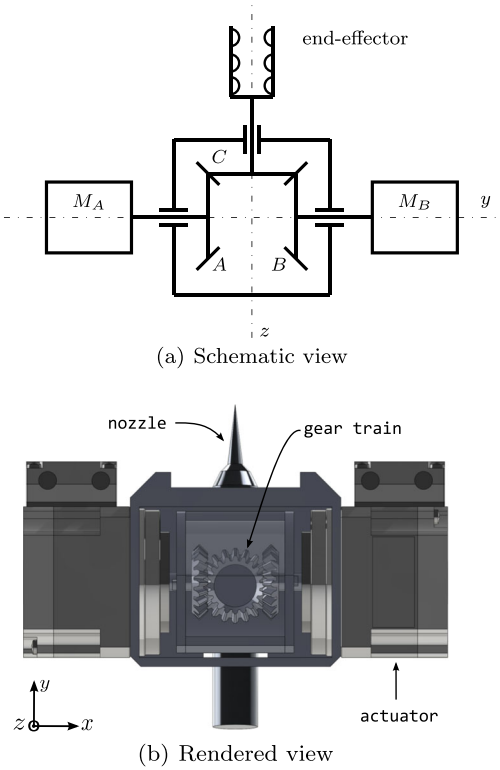

Fig. 5 The 2-DoF mechanism for the orientation of the nozzle (end–effector) inside the radome

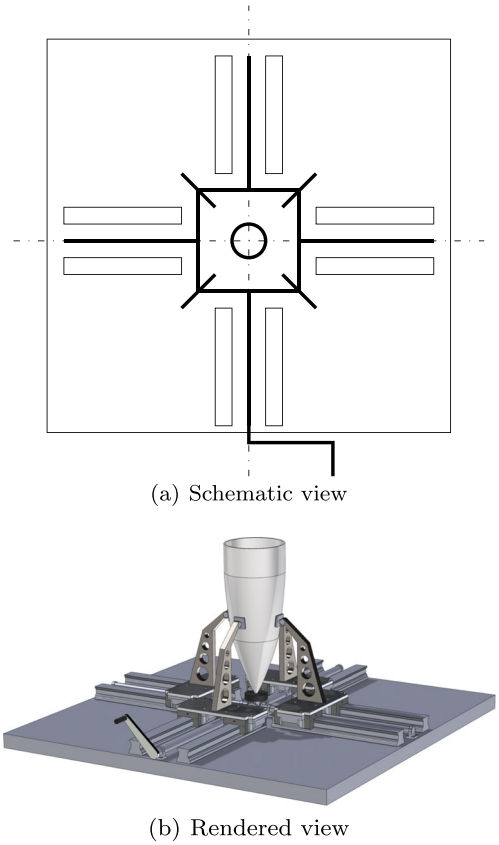

Fig. 6 The fixture system for the radome

and a toothed belt to increase the stiffness of the elongated structure. The compact 2–DoF orientation mechanism is designed using an epicyclic gear train transmission, made up of three identical gears A, B, and C, as illustrated in Fig. 5. The mechanism allows two rotations around two orthogonal axis, z and y, thanks to the motion provided by two electric actuators M_A and M_B, which move synchronized. This solution has been chosen for its simplicity, solidity as well as its stiffness, dexterity and ability to transport heavy payloads.

3.2 Fixture system

The fixture system for the radome has the objective of aligning its vertical axis with the vertical axis of the manipulator. Figure 6 shows the schematic and rendered views of the designed fixture. The system comprises four perpendicular ball screws which move four slides each one with a soft anchoring system, and a soft basis for the end–point of the radome. Each ball screw mounts a gear wheel in such a way that the rotation of one ball screws results into the rotation of all ball screws, with the same angle. The motion is generated from an external torque applied on a crank. Hence, by applying a torque on the crank, the four ball screws move each slide towards the radome, which results constrained in its vertical position.

4 Modeling

In this section, we report the inverse kinematics of the manipulator for mapping the reference trajectory given in the cartesian space (i.e., the FSS pattern) to the joint trajectories, since the control will be designed in the joint space. After, we compute the inverse dynamics for calculating the torques necessary to move the joints along the given trajectories.

4.1 Inverse kinematics

The prismatic joints of the manipulators have the objective to position the end effector in a point P of the workspace. Since the three translational axis are orthogonal, there is a 1:1 mapping between the 3D location of the point in the cartesian space and the stroke on the prismatic joints to get that point. However, as we can see from Fig. 3, we need to get that point with a particular orientation: indeed, the best deposition on a generic point P on the radome requires that the vertical axis of the nozzle is orthogonal to the tangent at point P. Algorithm 1 illustrates the inverse kinematics algorithm that we used for computing the orientation of the robotic system, namely the angle θ_y and θ_z for the 2–DoF compact wrist mechanisms.

Algorithm 1 Inverse kinematics computation

Require: $\mathbf{P}_i$=[x_i; y_i; z_i], $\mathbf{P}_{i-1}$=[x_{i-1}; y_{i-1}; z_{i-1}], $\mathbf{P}_{i+1}$=[x_{i+1}; y_{i+1}; z_{i+1}].
$\theta_z \leftarrow \text{atan}(y_i, x_i)$
$X \leftarrow R_{\theta_z}(:, 1) \cdot P_i$
$Y \leftarrow R_{\theta_z}(:, 2) \cdot P_i$
$\pm 1 \leftarrow \text{computeHalfplane}(Y)$
$0 \leftarrow z_{i-1}, z_{i+1}$
$0 \leftarrow y_{i-1}, y_{i+1}$
for all P_i **do**
  $z_{i-1}, z_{i+1} \leftarrow Zrad(i-1), Zrad(i)$
  $y_{i-1}, y_{i+1} \leftarrow Yrad(i-1), Yrad(i)$
end for
$m_1 \leftarrow \text{computeAngularCoefficient}(z_{i-1}, z_i, y_{i-1}, y_i)$
$m_2 \leftarrow \text{computeReciprocAngularCoefficient}(m_1)$
$\theta_y \leftarrow \text{computeSecAngle}(Halfplane, m_2)$

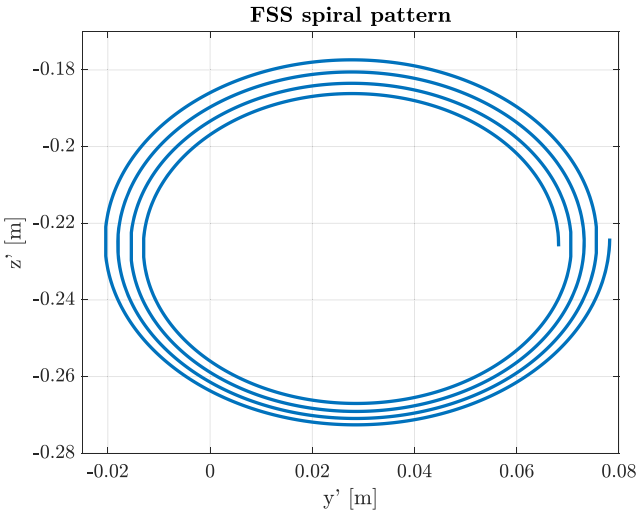

Fig. 8 FSS spiral pattern used in the simulations. See Fig. 4 for the position of the plane y'z' with respect to the radome reference frame Oxyz

4.2 Inverse dynamics

The dynamic analysis was performed using SimScape Multibody, a MATLAB/Simulink toolbox used to simulate the motion of rigid multibody systems. In this work, we do not consider flexibility effects [27, 28]. The SimScape solver constructs a system of differential algebraic equations (DAE) of motion where the bodies are modeled as rigid elements and the joints as algebraic constraints. The inverse dynamics of the non–controlled system consists of determining the joint torques (and forces) $\boldsymbol{\tau}(t)$ which are needed to generate the motion specified by the joint accelerations $\ddot{\boldsymbol{q}}(t)$, velocities $\dot{\boldsymbol{q}}(t)$, and positions $\boldsymbol{q}(t)$, obtained from the inverse kinematics computation. The mass and inertial parameters of the rigid bodies have been estimated from the CAD models of the manipulator. This analysis allows to size the parameters of the electric drives for the actuation of the joints.

4.3 Actuation

The actuation system for the considered scenario should have: (1) low inertia; (2) wide range of speed; (3) high positioning accuracy; (4) low torque ripple, so that also continuous rotations at low speeds are guaranteed.

The drive systems which guarantee the requirements are the electric DC brushless. The brushless DC servomotor consists of a rotating coil (rotor) which generates the magnetic flux, a stationary armature (stator) made by a polyphase winding and a static commutator that generates the feed sequence of the armature winding phases as a function of the rotor motion. From a modeling point of view, it can be described by a first–order transfer function between the armature voltage and current [29]. Indeed, in the domain of the complex variable s, the electric balance of the armature is described by the equations

$$\begin{cases} V_a = (R_a + sL_a)I_a + V_g & (1) \\ V_g = k_e \dot{q} & (2) \end{cases}$$

where V_a and I_a denote the armature voltage and current, R_a and L_a denote the armature resistance and inductance, V_g denotes the back electromotive force which is proportional to the angular velocity $\dot{q}$ of the joint through the electric constant k_e. The driving torque τ is obtained through the linear relashionship $\tau = k_m I_a$, where k_m is the mechanical constant which is numerically equal to k_e in the SI unit system for a compensated motor.

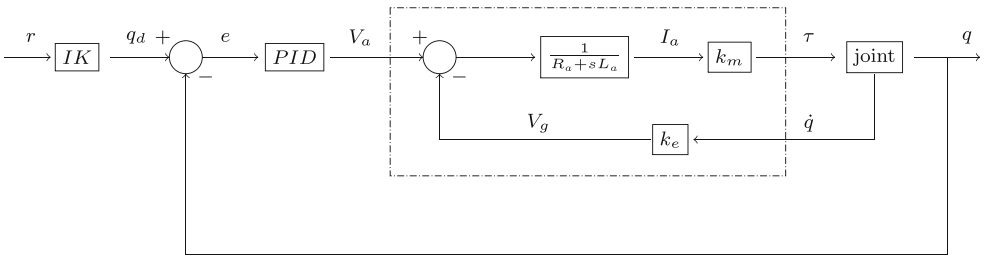

Fig. 7 The proposed system for controlling the motion of each joint of the manipulator

5 Control

The control system was designed in the joint space using a multivariable decentralized control structure. Each joint of the robot is controlled independently using a proportional–integral–derivative (PID) controller. This choice is motivated from the design of the mechanism, since the joints are kinematically uncoupled. Figure 7 shows all the components of the controlled mechanical system: the reference trajectory r corresponding to the FSS pattern that we want to achieve at the end–point of the manipulator, the inverse kinematics (IK) algorithm to map the reference trajectory given in the cartesian space to the desired positions q_d in the joint space, the PID controller, the mathematical model of the actuators previously described and the mechanical system. The input for each joint of the mechanical system is a torque τ, while the output is the position q of the joint itself.

6 Simulation

In this section, we describe the simulation of the motion control of the robotic manipulator along the joint trajectories which allow the nozzle to perform an additive manufacturing task inside the radome. The objective of the simulation is to show if the independent joint control architecture is able to guarantee the position accuracy required for the metal coating application. The robotic system should reach every point of the internal surface of many radome systems, according to the requirements from our industrial partner. To show the robustness of the design solution with respect to the many radome systems, we show the motion control of the robot in the worst case scenario, i.e., the internal surface of the radome with the smaller value of radius r and higher value of height h (see, e.g., Fig. 4). About the trajectory in the cartesian space, we consider the end–point of the nozzle following a spiral path. This trajectory was chosen to permit the direct writing of a spiral FSS pattern on the internal surface of the radome (see, e.g., Figs. 8 and 4). This particular pattern was chosen as illustrative example: indeed, the real FSS patterns are the sole property of our aerospace industrial partner. It is assumed that the tickness uniformity on the curved surface is ensured by the continuous flow of the aerosol through the nozzle. The selection of the flow velocity goes beyond the scope of the paper, and thus it is assumed to be optimal.

6.1 Trajectory

The trajectories in the cartesian space were mapped in the joint trajectories through the geometric inverse kinematics algorithm presented in Algorithm 1. This step allows to enstabilish the joint positions that the robotic manipulator has to follow to describe the spiral path. The resulting joint trajectories articulates in three phases: (i) mechanism reaching the central point of the spiral in 5s; (ii) spiral path in 20s; (iii) mechanism reaching the initial condition in 5s. The overall trajectory lasts 30s. Notice that phases (i) and (iii) follow a trapezoidal velocity profile, which has been already used in the context of AJP [30].

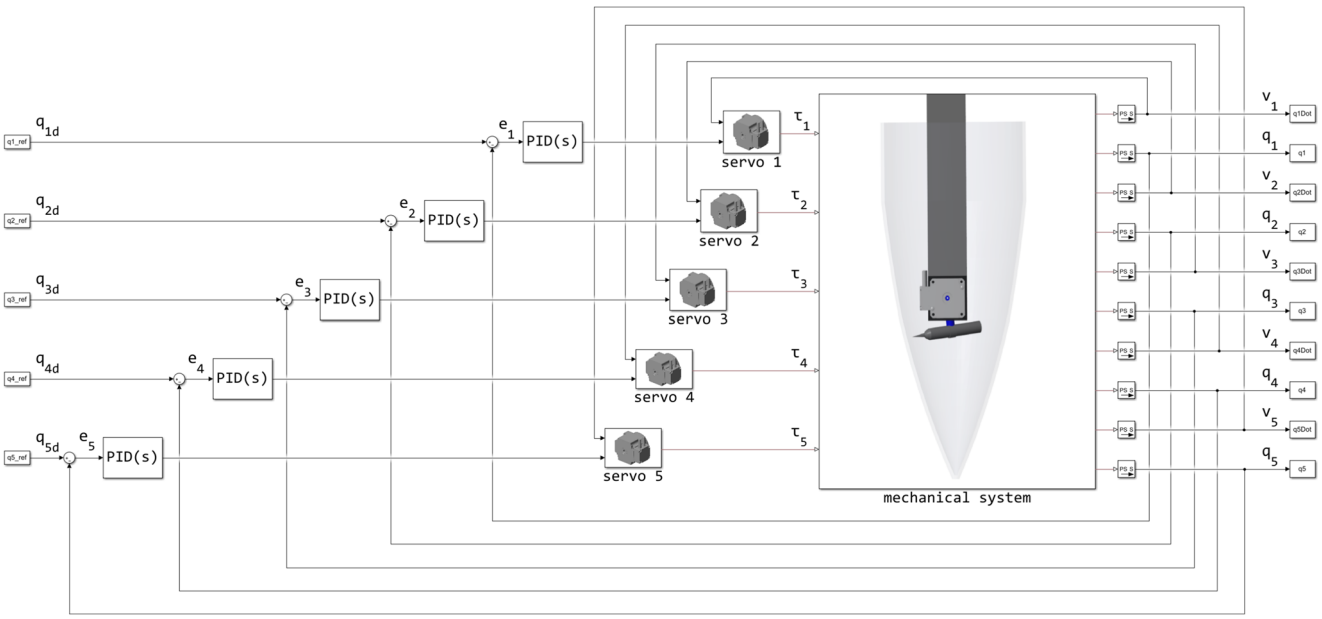

Fig. 9 A snapshot of the controlled system in MATLAB/Simulink. Starting from the left: q_{id} = desired joint trajectory; e_i = errors; τ_i = computed torques for each joint; q_i = actual joint position; v_i = actual joint velocity

Table 1 Electric drive parameters for the actuators of the 5-DoF manipulator. P = prismatic joint; R = rotational joint

	R_a [Ω]	L_a [10^{-5}H]	k_m [Nm/A]	k_e [rad/sV]
P	0.07	6	0.029	0.029
R	1.34	18	0.004	0.004

6.2 Simulation setup

The simulation was performed using MATLAB/Simulink. The gains of the PID controllers were tuned using the control system tuner available in Simulink. The system was numerically solved using a stiff second–order Runge–Kutta time integration scheme (by means of the *ode23s* function) with variable–step size. Figure 9 shows the simulation framework implemented in MATLAB/Simulink. From the left, we can notice the reference trajectories for the five joints q_{id}, already mapped from the reference trajectory described in the previous subsection, the five errors e_i, the five PID controllers, the five actuators, the five input torques for the mechanical system and, finally, the state of the manipulator, i.e., the actual joint positions and velocities. Notice that under the subsystems *servo* we can find an implementation of the actuation systems according to Eqs. 1–2. Table 1 reports the electric drive parameters of the actuators computed for ensuring the required prismatic and rotational motions. Indeed, under the subsystem *mechanical system* we can find the CAD models of the manipulator, directly imported as STL files into the simulation framework, as well as the joint connections between each component needed to generate the kinematical structure. Some snapshots of the simulations are illustrated in Fig. 10.

The simulation was performed on a Intel® Core™ i7-4910MQ CPU (quad-core 2.50 GHz, Turbo 3.50 GHz), 32 Gb RAM 1600MHz DDR3L, NVIDIA ®Quadro ®K2100M w/2GB GDDR5 VGA machine.

6.3 Results and discussion

We simulate the motion of the controlled system while performing the reference trajectory in the operative space given in Section 6.1, and we record the position errors at the joint level given by the difference between the reference joint position and the actual joint position (see e.g. Fig. 7 or Fig. 9), for 35s. A video of the simulation can be found here: https://www.youtube.com/watch?v=4Z8suJhoMUs. Figure 11 shows the position errors: all the controlled joints present an almost perfect

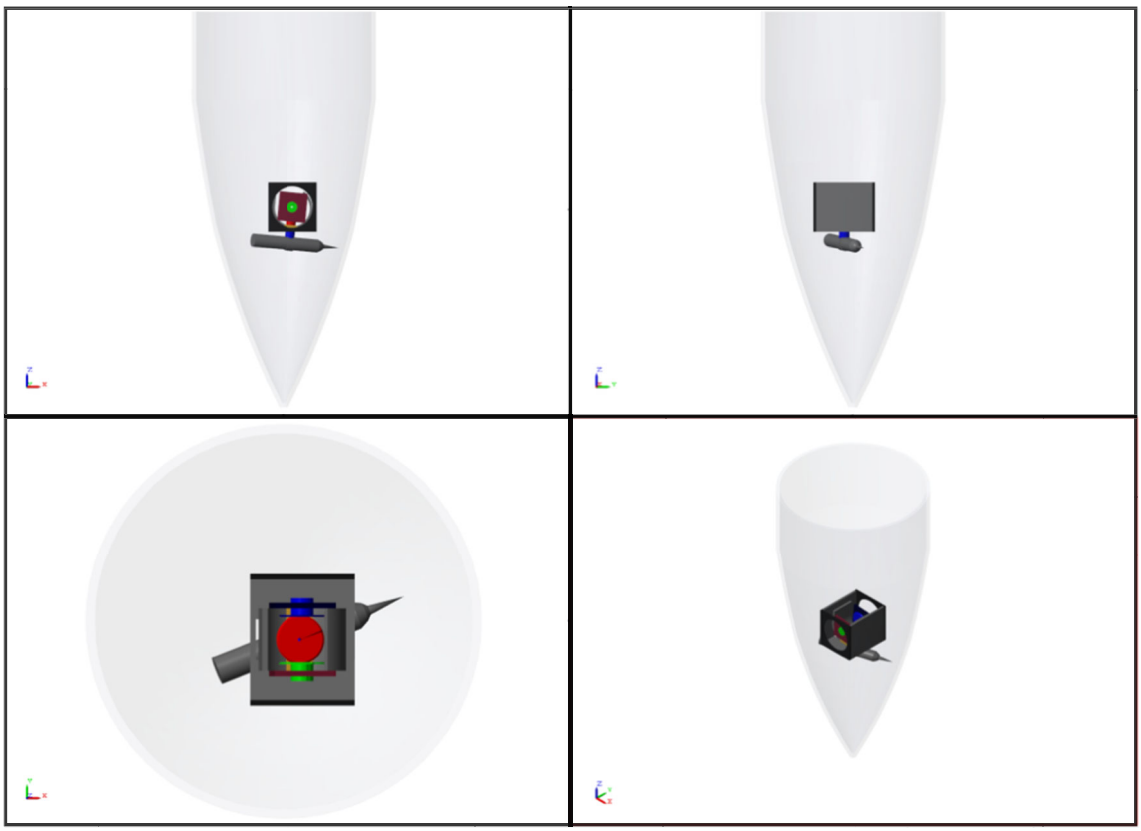

Fig. 10 Snapshots of the simulation. Views in the three planes and isometric view

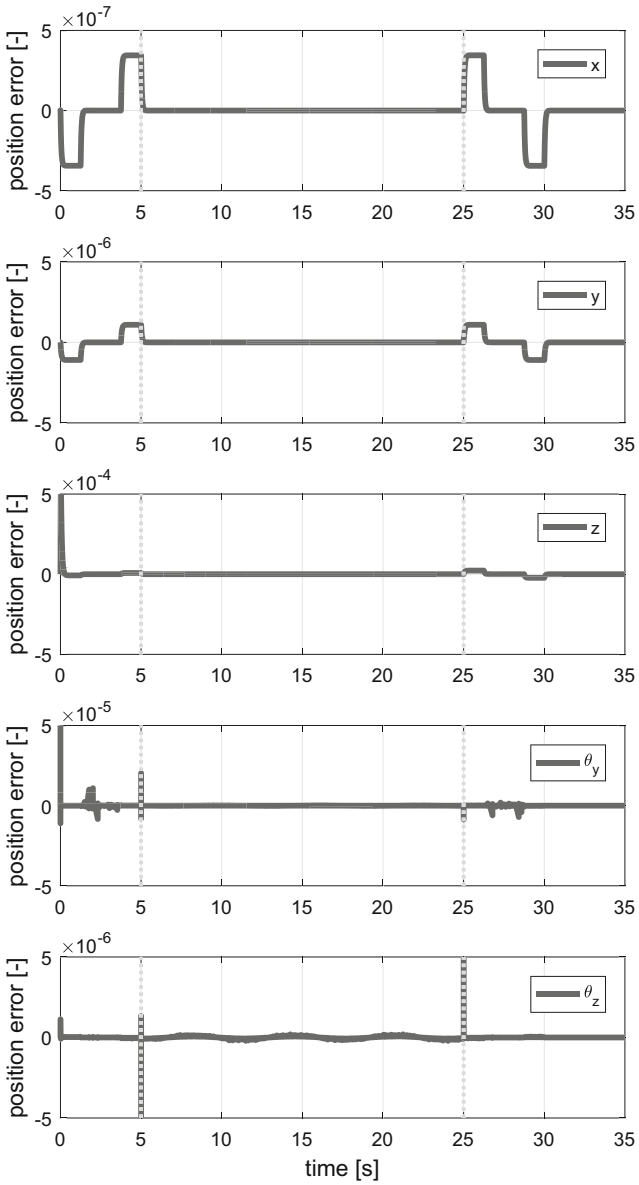

Fig. 11 Position errors of the five joints along the joint trajectories which allows to positionate the mechanism inside the radome, print the FSS spiral pattern in the plane $y'z'$, and returning to the initial position. The vertical dotted lines separate the three parts of the trajectory. Starting from the top: e_1, e_2, e_3, e_4, e_5

tracking. The errors are below the initial requirements of 10^{-3}. In these plots, we can notice the three phases of the joint trajectories. The mechanism reaches the worst case point of the internal surface of the radome in the first 5s. From here, the nozzle follows the spiral path in the plane tangent to the radome at that point (plane $y'z'$) till 25s, and after the mechanism reaches again its home configuration at the temporal instant 30s. Therefore, the independent joint control architecture might be able to guarantee the position accuracy requirements for robotic mechanisms in aerosol jet printing manufacturing processes. However, the implementation on real hardware might require, in addition to the current strategy, a method to suppress undesired vibrations [31] which can eventually arise at high frequency.

7 Conclusions

In this paper, we have presented a novel robotic mechanism for metal coating applications on curved surfaces. Due to the difficulty to coat a non-planar substrates, we have selected the aerosol jet printing as direct additive manufacturing technology for metal coating the internal surface of radome systems with FSS patterns. This choice is the starting point to design custom robotic solutions, since it provides the design requirements and specifications for the robotic system. In order to simplify the control of the device, we developed the robotic system as simple as possible from the mechanical point of view. Indeed, since the joints of the mechanisms are naturally decoupled, we proposed to use an independent joint control architecture where each joint is controlled independently, using a PID controller acting on the tracking error along the trajectory. This choice allowed to obtain position errors for the five joints far below the initial requirement of errors below 10^{-3}.

The design methodology adopted in this work is focused on aerosol jet printing processes. However, due to its generality, it can be adopted to other manufacturing processes. Indeed, the approach presented in this paper, which includes the mechanical design, the dynamical analysis and the control system design in the same simulation framework, makes it attractive in the development of complex mechatronic systems for manufacturing applications.

Further studies of the authors will be focused on the computer simulation of the aerosol jet beam impacting on the radome substrate, while the robotic nozzle moves on the three-dimensional space according to the controlled motion used in this study. The current work will be used as starting point for the future work of manufacturing the physical proof-of-concept for printing the FSS pattern on the internal surface of the radome system.

Acknowledgments This work was supported by the SIRena project, which has received funding from MISE, the Italian Ministry of Economic Development.

References

1. Mortara L, Hughes J, Ramsundar PS, Livesey F, Probert DR (2009) Proposed classification scheme for direct writing technologies. Rapid Prototyp J 15(4):299–309

2. Gibson I, Rosen DW, Stucker B et al (2010) Additive manufacturing technologies, volume 238, Springer, Berlin
3. Kadekar V, Fang W, Liou F (2004) Deposition technologies for micromanufacturing: a review. J Manuf Sci Eng 126(4):787–795
4. Dababneh AB, Ozbolat IT (2014) Bioprinting technology: a current state-of-the-art review. J Manuf Sci Eng 136(6):061016
5. Yee JS (1993) Frequency selective surface (fss), May 4, US Patent 5,208,603
6. Verde F, Scaglione A, Darsena D, Gelli G (2015) An amplify-and-forward scheme for spectrum sharing in cognitive radio channels. IEEE Trans Wirel Commun 14(10):5629–5642. https://doi.org/10.1109/TWC.2015.2440359
7. Darsena D, Di Vigilio L, Gelli G, Verde F (2015) Widely-linear frequency-shift compensation of CFO and I/Q imbalance in OFDMA/SC-FDMA systems. In: IEEE international conference on communications (ICC), IEEE, pp 2686–2691
8. Signore R, Grazioso S, Fariello A, Murgia F, Selvaggio M, Di Gironimo G (2017) Conceptual design and control strategy of a robotic cell for precision assembly in radar antenna systems, vol 11, pp 397–404. https://doi.org/10.1016/j.promfg.2017.07.123
9. Davis JR et al (2004) Handbook of thermal spray technology ASM international
10. Pawlowski L (2008) The science and engineering of thermal spray coatings. Wiley, New York
11. Mattox DM (2010) Handbook of physical vapor deposition (PVD) processing William Andrew
12. Park J, Sudarshan TS (2001) Chemical vapor deposition, volume 2 ASM international
13. Hedges M, Marin AB (2012) 3d aerosol jet printing-adding electronics functionality to rp/rm. In: DDMC 2012 conference, pp 14–15
14. Beyer C (2014) Strategic implications of current trends in additive manufacturing. J Manuf Sci Eng 136(6):064701
15. Bahnini I, Rivette M, Rechia A, Siadat A, Elmesbahi A (2018) Additive manufacturing technology: the status, applications, and prospects. The International Journal of Advanced Manufacturing Technology 97:147–161. https://doi.org/10.1007/s00170-018-1932-y
16. Goh GL, Agarwala S, Goh GD, Tan HKJ, Zhao L, Chuah TK, Yeong WY (2018) Additively manufactured multi-material free-form structure with printed electronics. Int J Adv Manuf Technol 94(1-4):1309–1316. https://doi.org/10.1007/s00170-017-0972-z
17. Hon KKB, Li L, Hutchings IM (2008) Direct writing technology - advances and developments. CIRP Annals Manuf Technol 57(2):601–620
18. Hoey JM, Lutfurakhmanov A, Schulz DL, Akhatov IS (2012) A review on aerosol-based direct-write and its applications for microelectronics. Journal of Nanotechnology 2012:1–22
19. Renn MJ (2014) Aerosol jet printed thin film transistors. Optomec Aerosol Jet White Paper
20. Hoey JM, Akhatov IS, Swenson OF, Schulz DL (2009) Convergent-divergent-convergent nozzle focusing of aerosol particles for micron-scale direct writing, February 26 US Patent App. 12/192,315
21. Goth C, Putzo S, Franke J (2011) Aerosol jet printing on rapid prototyping materials for fine pitch electronic applications. In: IEEE 61st electronic components and technology conference (ECTC), IEEE, pp 1211–1216
22. Espalin D, Muse DW, MacDonald E, Wicker RB (2014) 3d printing multifunctionality: structures with electronics. Int J Adv Manuf Technol 72(5-8):963–978
23. Sun H, Wang K, Li Y, Zhang C, Jin R (2017) Quality modeling of printed electronics in aerosol jet printing based on microscopic images. J Manuf Sci Eng 139(7):071012
24. Grazioso S, Selvaggio M, Marzullo D, Di Gironimo G, Gospodarczyk M (2017) Eligere: a fuzzy ahp distributed software platform for group decision making in engineering design. In: 2017 IEEE international conference on fuzzy systems (FUZZ-IEEE), IEEE, pp 1–6. https://doi.org/10.1109/FUZZ-IEEE.2017.8015713
25. Grazioso S, Gospodarczyk M, Di Gironimo G (2016) Distributed information systems in group decision making problems. In: 2016 fourth international conference on parallel, distributed and grid computing (PDGC), IEEE, pp 231–236
26. Kawabuchi I, Yoon WK, Kotoku T (2015) Linear-motion telescopic mechanism and robot arm having linear-motion telescopic mechanism, January 6, US Patent 8.925.405
27. Grazioso S, Sonneville V, Di Gironimo G, Bauchau O, Siciliano B (2016) A nonlinear finite element formalism for modelling flexible and soft manipulators. In: IEEE international conference on simulation, modeling and programming for autonomous robots (SIMPAR), IEEE, pp 185–190. https://doi.org/10.1109/SIMPAR.2016.7862394
28. Grazioso S, Di Gironimo G, Siciliano B (2018) A geometrically exact model for soft continuum robots: the finite element deformation space formulation. Soft Robotics. https://doi.org/10.1089/soro.2018.0047
29. Siciliano B, Sciavicco L, Villani L, Oriolo G (2010) Robotics: modelling, planning and control. Springer Science & Business Media, Berlin
30. Thompson B, Yoon H-S (2015) Velocity-regulated path planning algorithm for aerosol printing systems. J Manuf Sci Eng 137(3):031020
31. Grazioso S, Di Gironimo G, Singhose W, Siciliano B (2017) Input predictive shaping for vibration control of flexible systems. In: 2017 IEEE conference on control technology and applications (CCTA), IEEE, pp 305–310. https://doi.org/10.1109/CCTA.2017.8062480